Available online at www.sciencedirect.com

ScienceDirect

Energy Procedia 76 (2015) 17 – 26

Energy Procedia

European Geosciences Union General Assembly 2015, EGU

Division Energy, Resources & the Environment, ERE

Estimation of tidal stream potential in the Iroise Sea from velocity observations by High Frequency radars

Maxime Thiébaut[a], Alexei Sentchev[a]

[a]*Laboratoire d'Océanologie et de Géosciences (CNRS UMR 8187), Université du Littoral - Côte d'Opale, Wimereux 62930, France*

Abstract

A year-long surface current velocity time series recorded by High Frequency radars (HFR) are used for assessing the hydrokinetic resources at a near-shore site in the Iroise sea. A combination of remotely sensed surface velocities and ADCP velocity profiles recorded in radar coverage zone allowed assessing the tidal current variability and power density variations in three dimensions. The analysis revealed two areas with high energy potential: the Fromveur Strait and the area NW of the Ushant Island where the kinetic power density in the surface layer attains 1.5 kW/m^2. The power available in the bottom layer is 3 times lower.

Peer-review under responsibility of the GFZ German Research Centre for Geosciences

Keywords: Tidal stream potential, Hydrokinetic energy, Tidal currents circulation, HF radar, Iroise Sea

1. Introduction

The increase in global demand for electricity, especially in the densely populated countries, is expected to continue. In recognition of the pollution generated from fossil fuels many countries have pledged their commitment to reduce greenhouse gas emissions. Tidal stream energy, will play an important role in reducing these emissions. The European Union and its member states are currently setting targets for renewable energy generation. Generally, the kinetic energy of seawater caused by the rise and fall of the tides is in most places too low to provide a viable energy resource. However, in certain places a combination of the seabed bathymetry and the shape of coastline is such that tidal flows are concentrated and attain velocities that could provide cost-effective power generation. In many cases these velocities are sufficient to generate an unusually intense renewable energy resource, often ten times more than energy concentration available at a highly rated wind energy site. Moreover, a major advantage to be gained from utilization of this resource is that the energy availability is not dependent on weather variations, but has the accurate predictability of tidal movement.

Presently, the tidal-stream energy industry is in the early stage of development. Among the most advanced project

* Maxime Thiébaut. Tel.: +33-3-21-99-64-17; fax: +33-3-21-99-64-01.
E-mail address: maxime.thiebaut@univ-littoral.fr

Peer-review under responsibility of the GFZ German Research Centre for Geosciences
doi:10.1016/j.egypro.2015.07.835

they are: the 400 MW MeyGen facility in the Pentland Firth (UK) and the 300 MW OpenHydro in the Bay of Fundy (Canada) which holds the highest tidal range in the world and represents a major tidal energy resource.

Resource characterization is the first step towards a successful site selection and turbine deployment [1]. In earlier studies, tidal current velocity data from Admiralty Charts have been used to estimate tidal current energy resources [2]. However these estimates suffered from lack of precision. The use of old data survey, not originally intended for resource assessment are known to generate large prediction errors [3].

Underway velocity measurements by the towed or vessel mounted ADCP (Acoustic Doppler Current Profiler) is another efficient tool for tidal flow characterization and energy resource quantification. In the recent studies [4] velocity profiles were recorded while the vessel steamed around a circuit with sufficient frequency allowing to resolve the vertical structure of the tidal current and its spatial irregularities. Gooch et al. [5] used spatial interpolation of underway ADCP data to reconstruct a general tidal flow pattern neglecting the tidal phase difference during the surveying period. Goddijn-Murphy et al. [4] showed that the accuracy in reconstruction of the full 4-dimensional tidal flow can be significantly increased by merging observed velocities with the dynamical constraints provided a numerical model. In the absence of spatial coverage with observations, point measurements of velocity by ADCP or Acoustic Doppler Velocimeter (ADV) represent a unique opportunity of resource quantification from in situ data [6].

However, the resource quantification cannot be reduced to identification of regions with high current velocities. A wide range of factors have to be considered, especially temporal and spatial variability of the energy potential [7]. Although, ADCP and ADV have shown their effectiveness, notably with the estimation of turbulence [6] or to hydrodynamic models validation [8], they do not turn out sufficient to the spatial coverage of a study area. In contrast, numerical modeling of coastal circulation appeared as a powerful tool for hydrokinetic potential mapping. It allowed a considerable improvement in the quality of velocity and available power estimation. Nowadays, 3D models are routinely applied for tidal energy site assessment, resource quantification, and studies of the impact of energy devices on the local circulation and environment [1,9].

In this study, we present a new and very promising technique of site assessment based on the analysis of velocity data recorded by High Frequency radars (HFRs). We focus the analysis on power estimation around the Ushant Island, a region of high potential. As the HF radars measure only the surface current velocity, the knowledge of velocity profile is an important issue for site assessment. In this work, we supplement surface velocity observation set with velocity time series recorded by an ADCP in radar coverage zone. A power law was used to best fit the ADCP data and characterize the horizontal velocity variation with depth. A combination of remotely sensed surface velocity and ADCP velocity profiles allowed performing the analysis of tidal current variability in three dimensions and thus assessing energy resources in the most efficient way.

2. Data and methods

2.1. HFR data

A system of two high-frequency Wellen Radars (WERA) operating at 12.4 MHz has been deployed on the western Brittany coast since July 2006. Individual radar sites are located at Cape Garchine (site G), a seashore flat-ground area, and Cape Brezellec (site B), 50 km southward (Fig. 1). The radars measure the current velocity in the surface layer (0.7 m thick). The recorded radial velocities are the projections of the current velocity vector onto radar beam directions. In the present study, the radar network was configured to provide velocity estimates at high spatial resolution: 1.5 km along beam and 2^o azimuthal spacing, and time resolution of 20 minutes. The radial velocities measured by the two radars were interpolated on regular grid of 1 km spacing and combined to provide current vector maps. We used a powerful variational interpolation technique 2dVar [10], providing continuous velocity data on a regular grid within the area shown in Fig. 1 by grey shading. We generated 1.5 year-long velocity time series (04/2007 - 09/2008). A detail description of the experimental settings and methods of data processing of the radar network in the Iroise Sea can be found in [11].

2.2. ADCP data

A 600 kHz upward-looking RDI ADCP was deployed by the French Navy - SHOM (Service Hydrographique et Océanographique de la Marine) in the Fromveur Strait during 14 days, from March 19 to April 2, 1993. Velocities

were recorded at 0.2 Hz every 4 m, from 6 m to 52 m above the bottom. The deployment depth was 53 m. Given the strength of tidal currents in the Fromveur Strait, in situ data acquisition is very difficult and hazardous. In this sense, the ADCP measurements in 1993 represent unique data, and we decided to use them for comparison with radar velocity records. We selected a period from April 10, 2007 to April 23, 2007, for comparison and analysis of both ADCP and radar data. It is characterized by similar hydrodynamic conditions: spring season, secondary spring tide flow, and low wind.

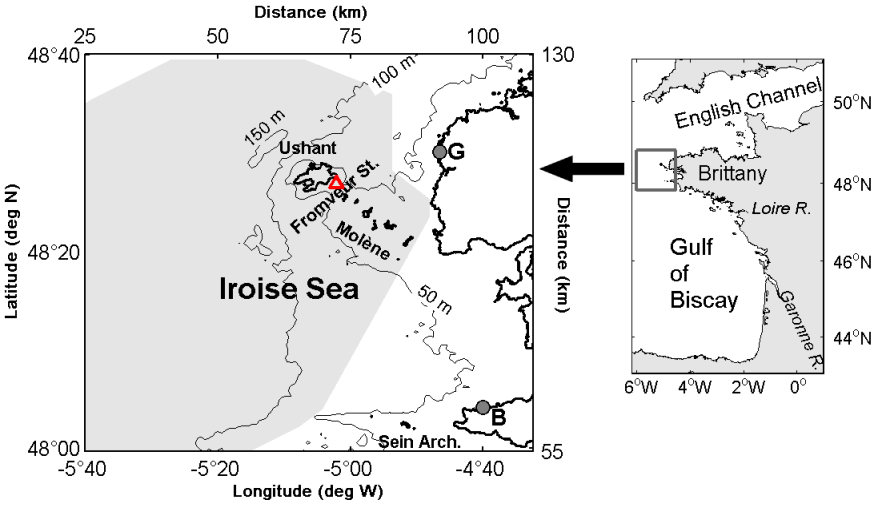

Fig. 1. Right panel: Location of the Iroise Sea and the HFR surveyed area (grey square). Left panel: Study area with radar coverage zone (grey shading), radar sites (grey circles), ADCP location (red triangle). Contour interval of the bathymetry is 50 m (grey solid lines). Geographic names used in the text are also shown.

2.3. Methods of analysis

2.3.1. Data analysis

We applied the Principal Component Analysis (PCA) [12] technique to HFR data set in order to quantify the tidal flow dynamics over a long period of observations. Parameters of synthesized ellipses, retrieved from the PCA, provide two major properties of tidal currents, direction and magnitude, and also indicate the tidal flow anisotropy. The latter is estimated as the ratio of eigenvalues of the velocity correlation tensor. We also applied a rotary analysis technique to velocity time series [12] in order to identify the ellipse polarization or the sign of current vector rotation: positive for counterclockwise (ccw) rotation and negative for clockwise (cw) rotation. Other analysis methods, such as harmonic, spectral, and statistical analysis, were applied to both radar derived velocities and ADCP data. EMEC proposed a list of significant parameters conventionally used for tidal energy screening. Among these metrics, we selected those which directly influence power estimation: the current strength and the asymmetry of velocities.

2.3.2. Metrics

Current strength characterization involves an assessment of the maximum, time averaged velocity, and also asymmetry of the tidal flow. The mean velocity is the average of current velocity magnitudes over a long period including values around slack water. Moreover, the maximum sustained velocity represents the maximum current observed. This establishes design loads on device support structures and foundations.

Besides, tidal flow asymmetry describes the difference between minimum and maximum of velocity magnitude. An imbalance between the strength of flood and ebb current speeds can exist, generating a considerably more power production during a specific stage of the tide. We used the following expression to estimate the asymmetry $a =< V >_{flood} / < V >_{ebb}$, where brackets mean time averaging of the velocity magnitude on flood and ebb flow.

Surface current speed measured by HFR used to assess the available resource at a site by estimating the power

density for different tidal stage and in selected area. As the HFR measurements are particularly efficient for current monitoring, it is possible to evaluate the available power density at different spatial locations using the conventional formula $P = 0.5\rho C_P V^3$ [13]; where ρ is water density, V - current velocity and C_P - dimensionless power coefficient set to 0.59. To take into account velocity decrease with depth, a power law relation derived from the best fit of HFR to ADCP data in the Strait was used.

HFR data allows assessing only the surface current velocity. Generally the maximum velocities are observed near the surface and minimum values near the seabed. To determine a beneficial hub-height and optimize the turbine design, the knowledge of velocity profile is required. Velocity distribution in the water column is commonly approximate by the power law: $V(z) = V_0(z/d)^{1/\alpha}$ [14]. V_0 is the surface velocity, d is the bottom depth, z is the distance above the seabed, and α is an empirical coefficient estimated from linear regression fit of LogLog representation of velocity.

3. Results

3.1. Tidal current velocity and velocity occurrence distributions

Spatial and temporal variability of tidal currents can be quantified using the parameters of synthesized tidal current ellipses derived from the PCA. The results are summarized in Fig. 2. Tidal current ellipses represent the 7-day averaged circulation pattern for a mean spring tide period. Ellipse orientation clearly shows that the tidal wave arrives from the Gulf of Biscay and travels northeastward toward the English Channel. The length of ellipse's semi-axis provides information about the tidal current strength and indicates regions with most powerful flow: west of the Ushant Island and the Fromveur Strait.

White and grey ellipses in Fig. 2 mark the clockwise (cw) and counter-clockwise (ccw) rotating currents. In the majority of domain, currents are rotating clockwise (cw). The largest region of the ccw rotating currents is located south of Ushant and Molène Islands. Another specific area of ccw current rotation is located west of Ushant where the tidal current velocity attains its maximum value. Analysis of the year-long velocity time series provided by the

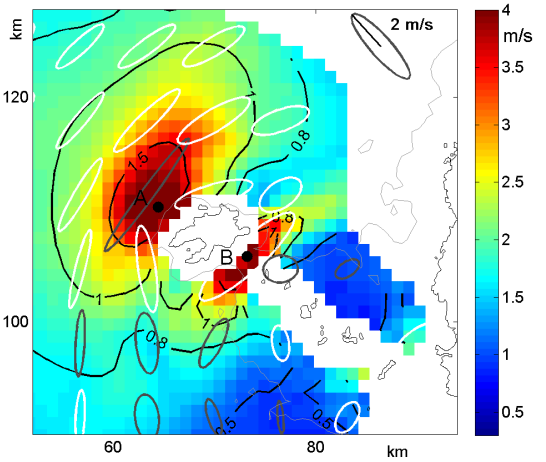

Fig. 2. Tidal current ellipses during spring tide (averaged over multiple spring tide periods during a year-long observations). Every sixth ellipse is shown. Grey ellipses denote counter-clockwise rotating tidal currents and white ellipses denote clockwise rotating currents. The maximum surface velocity during the study period (color shading) and spring tide average velocity (black contours). Letters *A* and *B* mark location of grid points where the highest velocities are observed.

radars allowed to identify areas with high flow potential and quantify the major parameters of the tidal flow. The maximum and time averaged current velocity distributions show significant spatial variations and ranges from 0.5 to 4 m/s for the maximum velocity and from 0.5 to 2 m/s for the mean velocity (Fig. 2). High bathymetry gradients in the north-eastern part of the study site and the presence of islands cause flow acceleration, tend to tighten the streamlines

and provide the maximum velocities west of Ushant Island and in the Fromveur Strait. In these two sectors, the annual mean velocity exceeds 1.5 m/s and the maximum attains 4 m/s.

Fig. 3 shows the annual cumulated occurrence of tidal current velocity in two grid points where the highest potential is expected (locations *A* and *B* in Fig. 2). It looks quite similar for both locations. The velocity value exceeds 1 m/s around 60% of time in both locations and 2 m/s more than 20% of time in the Fromveur Strait and 30% of time NW of Ushant Island.

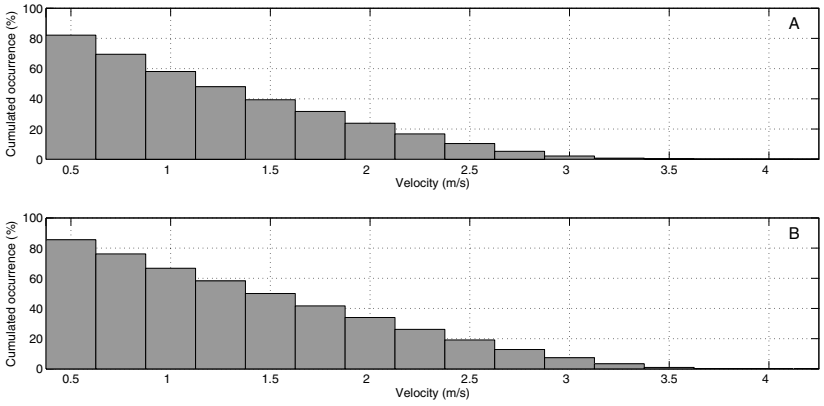

Fig. 3. Cumulative occurrence of velocity values in two particular locations (*A* and *B* in Fig. 2) where the highest velocities are observed.

3.2. Flow asymmetry

Although NW sector of the study area and the Fromveur Strait share certain properties of tidal currents, such as ellipse orientation, current strength and polarization, there is a noticeable difference between the two areas in the velocity asymmetry a (Fig. 4).

The asymmetry varies in a wide range, from 0.5 to 2.5, and shows spatial pattern with $a > 1$ in the West and $a < 1$ in the South. The strongest variation of asymmetry is observed in the Fromveur Strait. Here, the asymmetry values reach 2.5 in the onshore (northeastern) sector, indicating that flood flow velocities are by far higher than ebb flow velocities. The asymmetry decreases toward the centre of the Strait, where the tidal flow is balanced ($a = 1$). However, another distortion of velocity curve appears seaward, at the exit of the Strait. Here, and within an extended zone south of the Ushant Island, the asymmetry values decrease to 0.5 (Fig. 4) giving an evidence that the flow regime is ebb dominated. The asymmetry variability along the Fromveur Strait constitutes a remarkable phenomenon.

3.3. Velocity profiles

HFR data allows assessing only the surface current velocity. Generally the maximum velocities are observed near the surface and minimum values near the seabed. To determine a beneficial hub-height and optimize the turbine design, the knowledge of velocity profile is required. Using the ADCP data collected in the radar coverage zone, we reconstructed a time-average velocity profile for ebb and flood flow in the Fromveur Strait and compared it with the time average radar derived surface velocity in the nearest grid point. The results are shown in Fig. 5. We considered only the flood and ebb flow profiles where the depth average velocity exceeded 1 m/s. From the individual profiles, the time average profile was estimated for each stage of the tidal flow, and then approximated by a power law function of the form: $V(z) = V_0(z/d)^{1/\alpha}$, which is routinely used in oceanographic studies [5] and in the wind energy industry [14]. Here V_0 is velocity at the surface, z/d is the ratio of vertical level to bottom depth, and α is power coefficient. The best fit was obtained for $\alpha = 5.8$ for both profiles.

Extrapolation of the mean velocity profile in the surface layer revealed a very good agreement between time averaged ADCP and radar derived velocity values (Fig. 5). The relative error does not exceed 3%. However the overall variability of radar velocity (std) was larger. This is not surprising as wind and waves also contribute to total currents

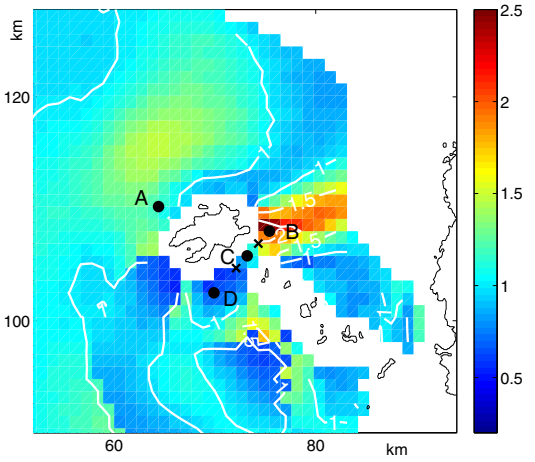

Fig. 4. Current velocity asymmetry distribution. Black circles show grid locations A and B selected for detailed analysis. Black crosses show locations of the grid points B_s and B_n, nearest to B, that were also selected for analysis.

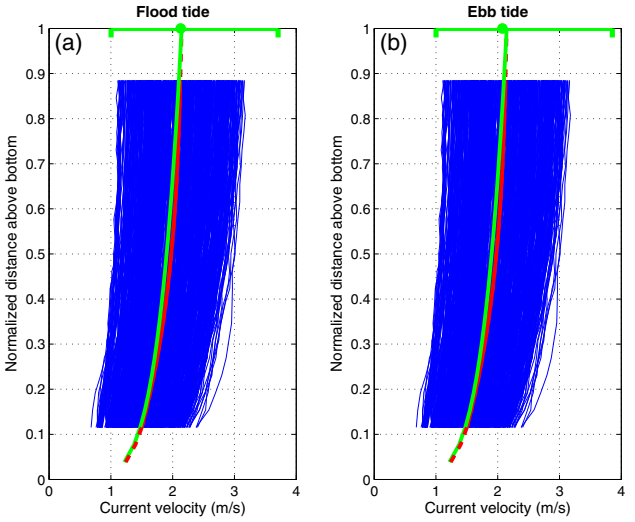

Fig. 5. Current velocity profiles (blue) during flood (a) and ebb (b) tide flow derived from ADCP measurements in the Fromveur Strait. The ADCP location are shown by the red triangle in Fig. 1. Average velocity profiles for both tidal stages are shown in red. Green curve represents the best fit of average velocity profile by a power law. Green point shows the mean value of surface current velocity derived from the radar measurements. Green ticks mark line matches the interval of velocity variations for each location and each stage of the tidal flow.

measured by the radars. Comparison of the radar derived and the depth averaged ADCP velocity time series in the ADCP location (Fig. 6) revealed a very good overall agreement with zero phase lag and high correlation (0.82) indicating that the radars tend to overestimate the depth averaged velocity by approximately 20%. The estimated ratio of depth averaged to surface velocity is 0.78. These values are in close agreement with the value 0.8 documented by [15] in the Dover Strait.

3.4. Hydrokinetic resources

It was assumed that the ADCP-derived velocity profile is representative for each grid point around the Ushant Island and along the Molène Island. The power density was estimated for different altitudes of device's deployment.

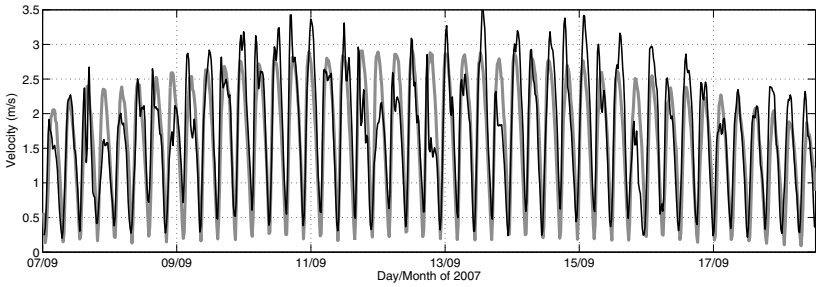

Fig. 6. Time series of the depth averaged velocity from ADCP measurements (grey) and surface current velocity recorded by the radars (black) in the grid point nearest to ADCP location.

Many types of devices are designed for deployment on the sea floor (e.g. Open Hydro, Sabella). Some are installed in the surface layer (e.g. Hydro-Gen, Evopod by Oceanflow). In the former case, it was assumed that rotating blades occupy the near bottom layer 15 m thick, where strong velocity shear occurs. Using the radar velocity times series, the power law expression for velocity profile ($\alpha = 5.8$), and the layer extension, velocity values were averaged to generate the power density time series in the surface and bottom layers. Since power density varies with the cube of velocity, the mean annual power density cannot be obtained by substituting the mean current speed into the above power density equation. Once the time variation of velocities is known for each point of the regular grid, the distribution of power densities can be readily calculated and averaged to find the mean annual power density [3].

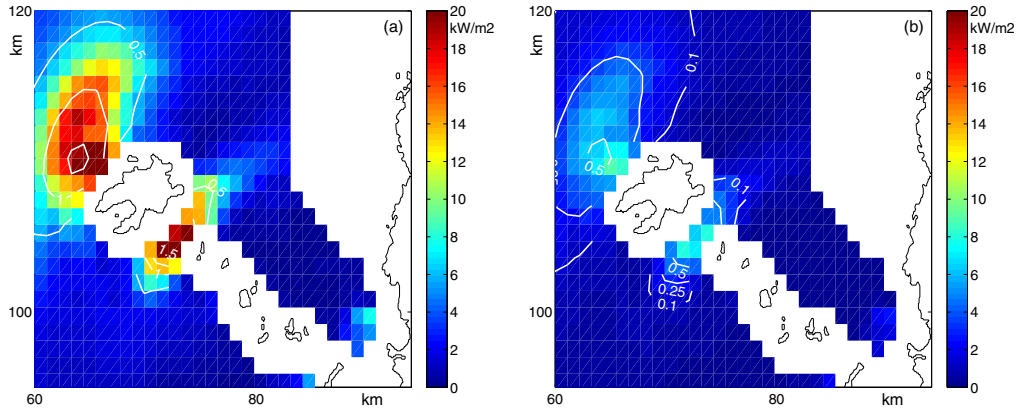

Fig. 7. Maximum (color shading) and mean annual (white contours) kinetic power density available in the surface (a) and bottom (b) layers.

Power density available around the Ushant Island in the surface and bottom layers are presented in Fig. 7. The maximum and time averaged power density distributions show significant spatial variations and ranges from 0.5 to 20 kW/m^2 for maximum power density and from 0.5 to 1.5kW/m^2 for the mean power density in the surface layer (Fig. 7a). High current velocities observed NW of Ushant Island and in the Fromveur Strait (Fig. 2) generate a high hydrokinetic potential in these two areas. In the bottom layer (Fig. 7b), the power available is 3 times lower than that observed on surface, with maximum and mean power density ranging from 0.5 to 10 kW/m^2 and from 0.1 to 0.5 kW/m^2 respectively.

However, the hydrokinetic resource varies with the stage of the tide. Representative hourly and daily average kinetic power densities are shown in Fig. 8. Huge variability on the hourly and daily time-scale is evident. For the hourly average (Fig. 8ac), the semi-diurnal inequality is clearly apparent on either side of the strong tides which generates peak power densities around every 6 hours for both locations. For the daily average over a 25-day period (Fig. 8bd), we observe nearly two neap-spring tidal cycles.

In addition to Fig.8, the cumulative distribution of power density was computed in the surface and bottom layer

in A and B locations (Fig. 9). Only velocities exceeding 1.2 m/s were used for power estimation (the corresponding threshold for power is 0.5 kW/m^2). We remind that the velocity profile was reconstructed for high (> 1 m/s) current speed values (Fig. 5). The 1 kW/m^2 value is reached more than 40% of time, the mean power density is equal to 1.6 (Table 1) and the maximum power $P > 6$ kW/m^2 is observed 6% of time. In the bottom layer, the estimated power density distribution is very different. The 1 kW/m^2 value is reached 15% and 22% of time in locations A and B respectively, and the overall mean power does not exceed 0.5 and 0.6 kW/m^2. There is also a big difference in power generation during spring and neap tide and, to a lower extent, during ebb and flood tide flow (Table 1). In the

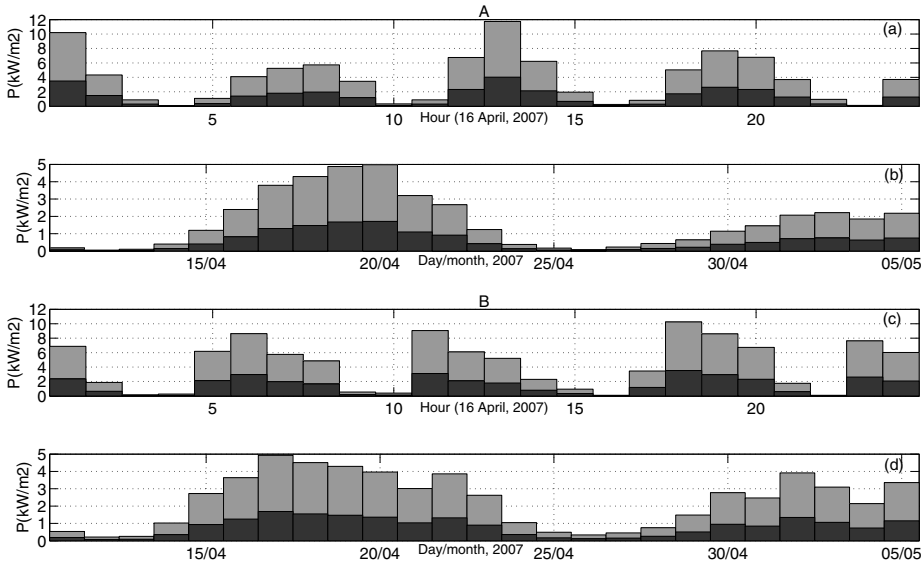

Fig. 8. Variations in average power density on an hourly (a,c) and daily (b,d) in locations A and B in the surface (grey) and bottom (black) layer.

Fromveur Strait, the power generation seems to be more balanced during the fortnight tidal cycle only in the central part at location B (variation from 0.7 to 2.2 kW/m^2). For other locations, further shoreward or seaward from B, more unbalanced power production is expected. Strong imbalance of power density is also documented in A. Our analysis indicates that in B_s, 1.4 km away from B, the mean power density is the highest: 1.8 kW/m^2 in the surface layer and 0.7 kW/m^2 in the bottom layer (Table 1). This difference in P is related to the ratio of surface to bottom layer velocities that is equal to 0.7 in the Fromveur Strait, and to 0.65 NW of the Ushant Island. Table 1 reveals that, for locations B and B_s, the power density is oppositely phased with respect to neap and flood tide flow. This is the consequence of velocity asymmetry which varies from 1 to 2 (Fig. 4).

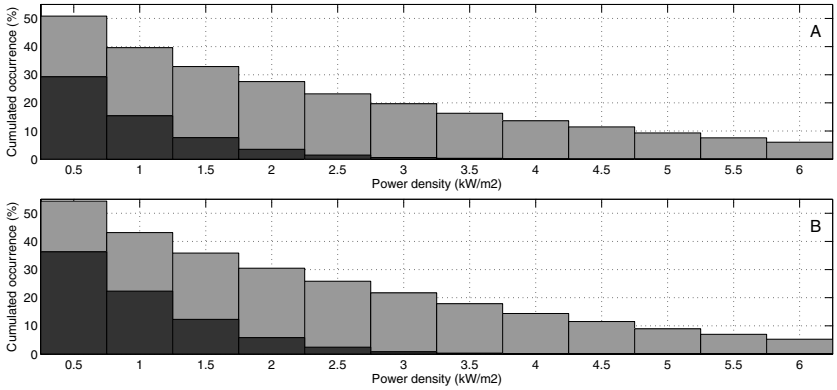

Fig. 9. Cumulative power density in the surface (grey) and bottom (black) layer, NW of Ushant Island (A) and in centre of the Fromveur Strait (B).

Table 1. Power density estimation (kW/m^2) in four particular locations (A, B, B_n and B_s) around the Ushant Island, for different stages of the tidal cycle and in two water layers (bottom and surface): average spring ($\overline{P_{spring}}$) and neap flow power ($\overline{P_{neap}}$), average ebb flow ($\overline{P_{ebb}}$) and flood flow power ($\overline{P_{flood}}$) in the surface layer ($\overline{P_{surface}}$) and bottom layer ($\overline{P_{bottom}}$) power density.

	$\overline{P_{spring}}$	$\overline{P_{neap}}$	$\overline{P_{flood}}$	$\overline{P_{ebb}}$	$\overline{P_{surface}}$	$\overline{P_{bottom}}$
A	2.8	0.3	1.9	1.5	1.6	0.5
B	2.2	0.7	1.8	1.3	1.6	0.6
B_n	1.4	0.3	1.5	0.2	0.9	0.3
B_s	2.6	0.7	1.1	2.2	1.8	0.7

In order to assess the effect of velocity asymmetry on power production we reconstructed power density time series from radar velocity records in three neighbouring grid points in the Fromveur Strait (B_n, B_s and B) during the spring tide (Fig. 10). The distance between two successive points is 1.4 km. The power density is strongly unbalanced during a day for B_n and B_s and much more balanced for B (Fig. 10). But if we aggregate tidal turbines deployed in B_n and B_s, the total power production during the period of interest could be much more balanced (Fig. 10b, grey shading), with the mean cumulative value of the order of 4 kW/m^2. Higher degree of balance of energy generation is achieved by exploiting the asymmetry variation in space.

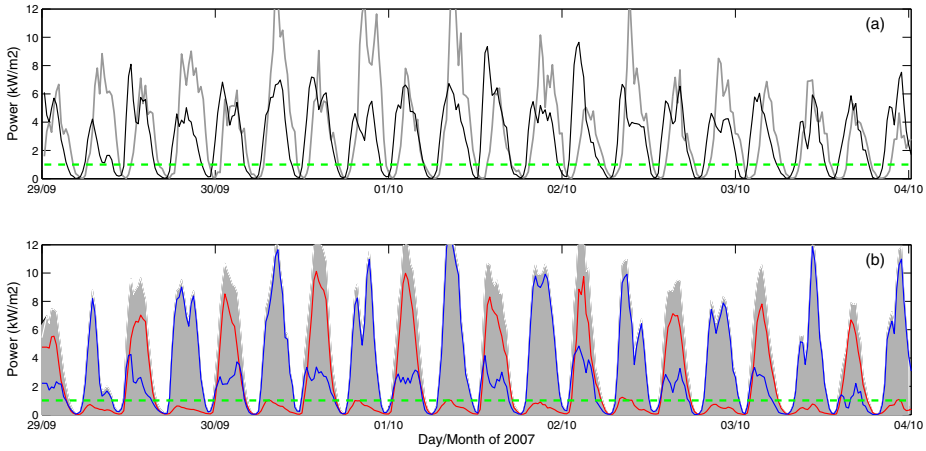

Fig. 10. (a) Power density P (kW/m^2) variation during a spring tide cycle in A (grey) and B (black). (b) P variation in B_n (red), B_s (blue), and a cumulative power density - sum of P in B_n and B_s (grey shading). Green line indicates the power density value of 1 kW/m^2.

4. Conclusion

An array of two HF radars, deployed on the W. Brittany coast since 2006, provides monitoring of the surface circulation in the Iroise sea in a large area extending up to 140 km offshore with high spatial and time resolution. We analyzed a year-long velocity time series and estimated the major metrics required for quantifying hydrokinetic resources of the tidal flow and their variations around the Ushant Island. We also compared radar derived velocities in the surface layer with velocity profiles recorded by an ADCP in the Fromveur Strait. This allowed quantifying variability of hydrokinetic resources in three dimensions.

The analysis revealed two areas with high energy potential particularly suitable for tidal stream device deployment: the Fromveur Strait and the area NW of the Ushant Island. The current velocity is higher than 4 m/s there, and time average velocity of 1 m/s is exceeded 60% of time on both sites. The mean spring tide current velocity attains 1.6 m/s and 1.7 m/s respectively. The map of maximum and mean velocity (Fig. 2) indicates that spatial extension of the former area is much bigger, while the area in the Fromveur Strait with extremely high velocity values does not exceed 6 x 2 km. Regarding the velocity variation with depth, a joint analysis of the radar derived and ADCP velocities in the Fromveur Strait shows that time average velocity profiles follow the power law. The best fit of the time average

velocity profiles provided the following values of the empirical constant $\alpha = 5.8$ for flood and ebb tide. Extrapolating ADCP velocity profile to the surface layer showed that the surface velocity estimate is very close to that derived from radar measurements (relative error 3%). Moreover, our results indicate that the ratio of depth averaged to surface velocity values is equal to 0.78 in the Fromveur Strait which is in close agreement with the ratio 0.8 documented by Prandle [15] in the Dover Strait, and also by Gooch et al. [5] in the Puget Sound, USA.

We analyzed the velocity asymmetry values, a, for typical spring, neap and mean tide conditions, revealed coherent spatial patterns, and documented variations of a in a wide range: from 0.5 to 2.5. The values $a > 1$ are found in the western sector of the study area, $a < 1$ in the southern sector and the strongest variation is observed in the Fromveur Strait. The hydrokinetic resources around the Ushant Island were estimated in the surface and bottom layers. NW of Ushant Island and in the Fromveur Strait the annually average kinetic power densities reach 1.5 kW/m^2 in the surface layer. The power available in the bottom layer is 3 times lower than that in the surface layer. A considerable resource variability on the hourly and daily time-scale has been diagnosed.

Finally, it was demonstrated that in the region of opposed flood- versus ebb-dominated asymmetries, occurring in the Fromveur Strait, it is possible to provide balanced power generation by aggregating devices and moving devices in space and to a different altitude above the bottom. This may help in searching solutions for turbine array configuration and optimizing power production by tidal power convertors.

Acknowledgments

The study was supported by the project PRO-TIDE of the Interreg IVB NW Europe program and represents a contribution to this project. ADCP data were provided by Ifremer and SHOM. We thank Louis Marié (Ifremer) for valuable information about these data. The HFR data were provided by ACTIMAR Company with the authorisation of the French Naval Oceanographic Centre (SHOM).

References

[1] Blunden, L.S., Bahaj, A.S.. Tidal energy resource assessment for tidal stream generators. Proceedings of the Institution of Mechanical Engineers, Part A: Journal of Power and Energy 2007;221(2):137–146.

[2] Black and Veatch, . PHASE II UK Tidal Stream Energy Resource Assessment. 2005.

[3] Hagerman, G., Polagye, B., Bedard, R., Previsic, M.. Methodology for estimating tidal current energy resources and power production by tidal in-stream energy conversion (TISEC) devices. EPRI North American tidal in stream power feasibility demonstration project 2006;1.

[4] Goddijn-Murphy, L., Woolf, D.K., Easton, M.C.. Current Patterns in the Inner Sound (Pentland Firth) from Underway ADCP Data*. Journal of Atmospheric and Oceanic Technology 2013;30(1):96–111.

[5] Gooch, S., Thomson, J., Polagye, B., Meggitt, D.. Site characterization for tidal power. In: OCEANS 2009, MTS/IEEE Biloxi-Marine Technology for Our Future: Global and Local Challenges. IEEE; 2009, p. 1–10.

[6] Thomson, J., Polagye, B., Durgesh, V., Richmond, M.C.. Measurements of turbulence at two tidal energy sites in Puget Sound, WA. Oceanic Engineering, IEEE Journal of 2012;37(3):363–374.

[7] Neill, S.P., Hashemi, M.R., Lewis, M.J.. The role of tidal asymmetry in characterizing the tidal energy resource of Orkney. Renewable Energy 2014;68:337–350.

[8] Carballo, R., Iglesias, G., Castro, A.. Numerical model evaluation of tidal stream energy resources in the Ría de Muros (NW Spain). Renewable Energy 2009;34(6):1517–1524.

[9] Lewis, M., Neill, S.P., Robins, P.E., Hashemi, M.R.. Resource assessment for future generations of tidal-stream energy arrays. Energy 2015;83:403–415.

[10] Yaremchuk, M., Sentchev, A.. A combined EOF/variational approach for mapping radar-derived sea surface currents. Continental Shelf Research 2011;31(7):758–768.

[11] Sentchev, A., Forget, P., Barbin, Y., Yaremchuk, M.. Surface circulation in the Iroise Sea (W. Brittany) from high resolution HF radar mapping. Journal of Marine Systems 2013;109:S153–S168.

[12] Thomson, R.E., Emery, W.J.. Data analysis methods in physical oceanography. Newnes; 2014.

[13] Houlsby, G.T., Draper, S., Oldfield, M.L.G.. Application of linear momentum actuator disc theory to open channel flow. Report no OUEL 2008;2296(08).

[14] Peterson, E.W., Hennessey Jr, J.P.. On the use of power laws for estimates of wind power potential. Journal of Applied Meteorology 1978;17(3):390–394.

[15] Prandle, D.. Year-long measurements of flow-through the dover strait by HF radar and acoustic doppler current profilers (ADCP). Oceanologica Acta 1993;16(5-6):457–468.